A&A 556, A15 (2013)
DOI: 10.1051/0004-6361/201321346

Astronomy & Astrophysics

The effective temperature scale of M dwarfs⋆

A. S. Rajpurohit[1], C. Reylé[1], F. Allard[2], D. Homeier[2], M. Schultheis[1,3], M. S. Bessell[4], and A. C. Robin[1]

[1] Institut UTINAM CNRS 6213, Observatoire des Sciences de l'Univers THETA Franche-Comté-Bourgogne, Université de Franche-Comté, Observatoire de Besançon, BP 1615, 25010 Besançon Cedex, France
e-mail: arvind@obs-besancon.fr
[2] Centre de Recherche Astrophysique de Lyon, UMR 5574: CNRS, Université de Lyon, École Normale Supérieure de Lyon, 46 allée d'Italie, 69364 Lyon Cedex 7, France
[3] Université de Nice Sophia-Antipolis, CNRS, Observatoire de Côte d'Azur, Laboratoire Cassiopée, 06304 Nice Cedex 4, France
[4] Research School of Astronomy and Astrophysics, Mount Stromlo Observatory, Cotter Road, Weston Creek, ACT 2611, Australia

Received 22 February 2013 / Accepted 12 April 2013

ABSTRACT

Context. Despite their large number in the Galaxy, M dwarfs remain elusive objects and the modeling of their photosphere has long remained a challenge (molecular opacities, dust cloud formation).
Aims. Our objectives are to validate the BT-Settl model atmospheres, update the M dwarf $T_{\rm eff}$-spectral type relation, and find the atmospheric parameters of the stars in our sample.
Methods. We compare two samples of optical spectra covering the whole M dwarf sequence with the most recent BT-Settl synthetic spectra and use a χ^2 minimization technique to determine $T_{\rm eff}$. The first sample consists of 97 low-resolution spectra obtained with New Technology Telescope (NTT) at La Silla Observatory. The second sample contains 55 medium-resolution spectra obtained at the Siding Spring Observatory (SSO). The spectral typing is realized by comparison with already classified M dwarfs.
Results. We show that the BT-Settl synthetic spectra reproduce the slope of the spectral energy distribution and most of its features. Only the CaOH band at 5570 Å and AlH and NaH hydrides in the blue part of the spectra are still missing in the models. The $T_{\rm eff}$ scale obtained with the higher resolved SSO 2.3 m spectra is consistent with that obtained with the NTT spectra. We compare our $T_{\rm eff}$ scale with those of other authors and with published isochrones using the BT-Settl colors. We also present relations between effective temperature, spectral type, and colors of the M dwarfs.

Key words. stars: atmospheres – stars: low-mass – stars: fundamental parameters

1. Introduction

Low-mass stars of less than 1 $M_\odot$ are the dominant stellar component of the Milky Way. They constitute 70% of all stars (Reid & Gizis 1997; Bochanski et al. 2010) and 40% of the total stellar mass of the Galaxy (Chabrier 2003, 2005). Our understanding of the Galaxy therefore relies upon the description of this faint component. Indeed, M dwarfs have been employed in several Galactic studies as they carry the fundamental information on the stellar physics as well as on the galactic structure, formation, and dynamics. Moreover, M dwarfs are now known to host exoplanets, including super-Earth exoplanets (Bonfils et al. 2007, 2012; Udry et al. 2007). The determination of accurate fundamental parameters for M dwarfs has therefore relevant implications for both stellar and Galactic astronomy. Because of their intrinsic faintness and difficulties in getting homogeneous samples with respect to age and metallicity, their physics is not yet well understood.

Historically, their atmosphere has been complex to model, with the need for computed and ab initio molecular line lists that are accurate and complete with high temperatures. But for over ten years, water vapor (Partridge & Schwenke 1997; Barber et al. 2006) and titanium oxide (Plez 1998) line lists, the two most important opacities in strength and spectral coverage, have become available and meet these conditions. Indeed, the PHOENIX model atmosphere synthetic spectral energy distribution (SED) has improved greatly from earlier studies Allard & Hauschildt 1995; Hauschildt et al. 1999) to the more recent models by Allard et al. (2001, 2011, 2012a) and by Witte et al. (2011) using the most recent water vapor opacities.

The $T_{\rm eff}$ scale of M dwarfs remains to this day model dependent to some level. Many efforts have been made to derive the effective temperature scale of M dwarfs. Due to the lack of very reliable model atmosphere, indirect methods such as blackbody fitting techniques have historically been used to estimate the effective temperature. The Bessell (1991) $T_{\rm eff}$ scale was based on blackbody fits to the near-infrared (NIR) $JHKL$ bands by Pettersen (1980) and Reid & Gilmore (1984). The much cooler blackbody fits shown by Wing & Rinsland (1979) and Veeder (1974) were fitted to the optical. Their fitting line was a continuation of the empirical $T_{\rm eff}$ relation for the hotter stars through the Pettersen (1980) and Reid & Gilmore (1984) NIR fits for the cooler stars. The work by Veeder (1974), Berriman & Reid (1987), Berriman et al. (1992), and Tinney et al. (1993) also used the blackbody fitting technique to estimate the $T_{\rm eff}$. Tsuji et al. (1996a) provide good $T_{\rm eff}$ using infrared flux method (IRFM). Casagrande et al. (2008) provide a modified IRFM $T_{\rm eff}$ for dwarfs including M dwarfs. These methods tend to underestimate $T_{\rm eff}$ since the blackbody carries little flux compared to the M dwarfs in the Rayleigh Jeans tail redwards of 2.5 μm. Temperatures derived from fitting to model spectra (Kirkpatrick et al. 1993) are systematically ~300 K warmer than

⋆ Tables 1 and 2 are available in electronic form at http://www.aanda.org

those attained by empirical methods. This cooler $T_{\rm eff}$ scale for M dwarfs was corrected recently by Casagrande & Schönrich (2012) bring it close to the Bessell (1991, 1995) $T_{\rm eff}$ scale.

Tinney & Reid (1998) determined an M dwarf $T_{\rm eff}$ scale in the optical by ranking the objects in order of titanium oxide (TiO), vanadium oxide (VO), CrH, and FeH equivalent widths. Delfosse et al. (1999) pursued a similar program in the NIR with H_2O indices. Tokunaga & Kobayashi (1999) used a spectral color index based on moderate dispersion spectroscopy in the K band. Leggett et al. (1996) used observed NIR low-resolution spectra and photometry for comparison with the AMES-Dusty models (Allard et al. 2001). They found radii and effective temperatures that are consistent with the estimates based on photometric data from interior model or isochrone results. Leggett et al. (1998, 2000) revised their results by comparing the SED and NIR colors of M dwarfs to the same models. Their study provided for the first time a realistic temperature scale of M dwarfs.

In this paper, we present a new version of the BT-Settl models using the TiO line list by Plez (1998) and Plez, priv. comm., which is an important update since TiO accounts for the most important features in the optical spectrum. Compared to the version presented in Allard et al. (2012a) that was using Asplund et al. (2009) solar abundances, this new BT-Settl model also employs the latest solar elemental abundances by Caffau et al. (2011). We compare the revised BT-Settl synthetic spectra with the observed spectra of 152 M dwarfs using spectral synthesis and χ^2 minimization techniques, as well as color–color diagrams to obtain the atmospheric parameters (effective temperature, surface gravity and metallicity). We determine the revised effective temperature scale along the entire M dwarfs' spectral sequence and compare these results to those obtained by many authors. Observations and spectral classification are presented in Sect. 2. Details of the model atmospheres are described in Sect. 3, and the $T_{\rm eff}$ determination is explained in Sect. 4. The comparison between observations and models is done in Sect. 5, where spectral features and photometry are compared. The effective temperature scale of M dwarfs is presented in this section. Conclusions are given in Sect. 6.

2. Observations

We carried out spectroscopic observations on the 3.6 mm New Technology Telescope (NTT) at La Silla Observatory (ESO, Chile) in November 2003. Optical low-resolution spectra were obtained in the red imaging and low-dispersion spectroscopy (RILD) observing mode with the ESO Multi Mode Instrument (EMMI) instrument. The spectral dispersion of the grism we used is 0.28 nm/pix, with a wavelength range of 385–950 nm. We used an order-blocking filter to avoid the second-order overlap that occurs beyond 800 nm. Thus the effective wavelength coverage ranges from 520 to 950 nm. The slit was 1 arcsec wide and the resulting resolution was 1 nm. The seeing varied from 0.5 to 1.5 arcsec. Exposure time ranged from 15 s for the brightest to 120 s for the faintest dwarf (I = 15.3). The reduction of the spectra was done using the context *long* of MIDAS. Fluxes were calibrated with the spectrophotometric standards LTT 2415 and Feige 110.

We obtained spectra for 97 M dwarfs along the entire spectral sequence. They are presented in Reylé et al. (2006), Phan-Bao et al. (2005), Crifo et al. (2005), and Martín et al. (2010). The list of stars, their spectral types, and their optical and NIR photometry are given in Table 1. The photometry has been compiled using the Vizier catalog access through the Centre de Données astronomiques de Strasbourg. It comes from the Naval Observatory Merged Astrometric Dataset (NOMAD) catalog (Zacharias et al. 2005), the Deep Near-Infrared Survey (DENIS, Epchtein 1997), and the Two Micron All Sky Survey (2MASS, Skrutskie et al. 2006), Reid et al. (2004, 2007), Koen & Eyer (2002); Koen et al. (2010).

The observations of 55 additional M dwarfs at Siding Spring Observatory (SSO) were carried out using the Double Beam Spectrograph (DBS), which uses a dichroic beamsplitter to separate the blue (300–630 nm) and red (620–1000 nm) light. The blue camera with a 300 l/mm grating provided a 2-pixel resolution of 0.4 nm, and the red camera with a 316 l/mm grating provided a 2-pixel resolution of 0.37 nm. The detectors were E2V 2048 × 512 13.5 micron/pixel CCDs. The observations were taken on Mar. 27 2008. The spectrophotometric standards used were HD 44007, HD 45282, HD 55496, HD 184266, and HD 187111 from the Next Generation Spectral Library (NGSL, version 1)[1] L745-46a and EG131 from `http://www.mso.anu.edu.au/~bessell/FTP/Spectrophotometry/`. The list of stars with their photometry are given in Table 2.

Spectral types for the NTT sample are obtained by visual comparison with a spectral template of comparison stars, observed together with the target stars at NTT as explained in Reylé et al. (2006). For comparison, we also derive spectral types using the classification scheme based on the TiO and CaH bandstrength (Reid & Gizis 1997). However, no comparison stars have been observed with the DBS at SSO. Thus, spectral types for the SSO sample are computed from TiO and CaH bandstrength. Although the instrument is different, we allow the comparison stars observed with EMMI on the NTT to be used as a final check. The results agree within 0.5 subclass.

3. Model atmospheres

For this paper, we use the most recent BT-Settl models, which are partially published in a review by Allard et al. (2012a) and described by Allard et al. (2012b). These model atmospheres are computed with the PHOENIX multi-purpose atmosphere code version 15.5 (Hauschildt et al. 1997; Allard et al. 2001) solving the radiative transfer in 1D spherical symmetry. The assumptions made are classical: hydrostatic equilibrium, convection using the mixing length theory, chemical equilibrium, and a sampling treatment of the opacities. The models use a mixing length as derived by the radiation hydrodynamic (RHD) simulations of Ludwig et al. (2002, 2006) and Freytag et al. (2012) and radius determined by the Baraffe et al. (1998) interior models as a function of the atmospheric parameters ($T_{\rm eff}$, $\log g$, [M/H]). The BT-Settl grid extends from $T_{\rm eff}$ = 300−7000 K, $\log g$ = 2.5−5.5, and [M/H] = −2.5−0.0 which accounts for alpha-element enrichment. The reference solar elemental abundances used in this version of the BT-Settl models are those defined by Caffau et al. (2011). The synthetic colors and spectra are distributed with a spectral resolution of around R = 100 000 via the PHOENIX web simulator[2].

Hot-temperature grains have been shown to form in the uppermost layers of M dwarfs with effective temperatures below 3000 K, but clear effects observable at the spectral resolution considered in this paper are only apparent below 2600 K, that is, for later spectral types than those considered in this paper.

[1] `http://archive.stsci.edu/prepds/stisngsl/index.html`
[2] `http://phoenix.ens-lyon.fr/simulator`

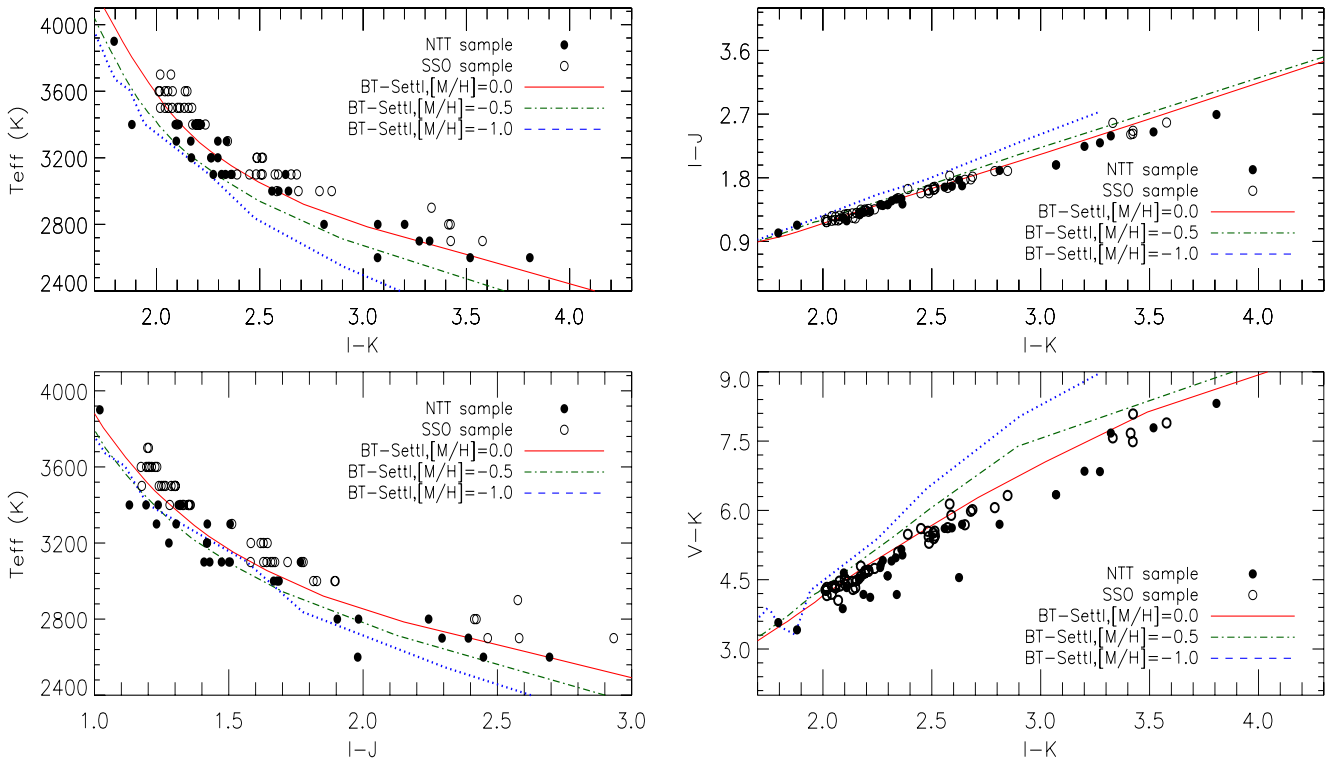

Fig. 1. $T_{\rm eff}$ vs. NIR colors (*left panel*) and color-color plot (*right panel*) for observed M dwarfs (open and filled circle) compared to the values obtained with the 5 Gyr isochrones from Baraffe et al. (1998) at various metallicities.

These grains produce a "veiling" by dust scattering over the optical band of the latest type M dwarfs. The BT-Settl models use therefore a slightly revised version of the Rossow (1978) cloud model (see Allard et al. 2012a,b; Rajpurohit et al. 2012b), for details on the model construction.

Compared to previous models by Allard et al. (2001), the current version of the BT-Settl model atmosphere is using the BT2 water vapor line list computed by Barber et al. (2006), TiO, VO, CaH line lists by Plez (1998), MgH by Skory et al. (2003), and Weck et al. (2003), FeH and CrH by Chowdhury et al. (2006) and Dulick et al. (2003), NH_3 by Yurchenko et al. (2011), CO_2 by Tashkun et al. (2004), and H_2 Collision Induced Absorption (CIA) by Borysow et al. (2001) and Abel et al. (2011), to mention the most important. We use the CO line list by Goorvitch & Chackerian (1994a,b). Detailed profiles for the alkali lines are also used (Allard et al. 2007).

In general, the Unsold (1968) approximation is used for the atomic damping constants with a correction factor to the widths of 2.5 for the non-hydrogenic atoms (Valenti & Piskunov 1996). More accurate broadening data for neutral hydrogen collisions by Barklem et al. (2000) have been included for several important atomic transitions, such as the alkali, Ca I and Ca II resonance lines. For molecular lines, we adopted average values (e.g., $\langle\gamma_6^{\rm HIT}(T_0, P_0{}^3)\rangle_{\rm H_2O} = 0.08\ P_{\rm gas}\ [\rm cm^{-1}\ atm^{-1}]$ for water vapor lines) from the HITRAN database (Rothman et al. 2009), which are scaled to the local gas pressure and temperature:

$$\gamma_6(T) = \left\langle \gamma_6^{\rm HIT}(T_0, P_0) \right\rangle \left(\frac{296\ \rm K}{T}\right)^{0.5} \left(\frac{P}{1\ \rm atm}\right), \quad (1)$$

with a single temperature exponent of 0.5 to be compared to values ranging mainly from 0.3 to 0.6 for water transitions studied by Gamache et al. (1996). The HITRAN database gives widths for broadening in air, but Bailey & Kedziora-Chudczer (2012) find that these agree in general within 10–20% with those for broadening by a solar composition hydrogen-helium mixture.

[3] Standard temperature 296 K and pressure 1 atm.

4. $T_{\rm eff}$ determination

We use a least-square minimization program employing the new BT-Settl model atmospheres to derive a revised effective temperature scale of M dwarfs. The stars in our samples most probably belong to the thin disc of our Galaxy (Reylé et al. 2002; Reylé & Robin 2004). Thus we determine the $T_{\rm eff}$ of our targets by assuming solar metallicity. This is a reasonable assumption, as can be seen in Fig. 1 where we compare our two samples to three 5 Gyr isochrones with solar, [M/H] = –0.5 and –1.0 dex. The samples are clearly compatible with solar metallicity.

Both theory and observation indicate that M dwarfs have $\log g = 5.0 \pm 0.2$ (Gizis 1996; Casagrande et al. 2008) except for the latest type M dwarfs. We therefore restrict our analysis to $\log g = 5.0$–5.5 models. Each synthetic spectrum was convolved to the observed spectral resolution; a scaling factor is applied to normalize the average flux to unity. We then compare each of the observed spectra with all the synthetic spectra in the grid by taking the difference between the flux values of the synthetic and observed spectra at each wavelength point. We interpolated the model spectra on the wavelength grid of the observed spectra. The sum of the squares of these differences is obtained for each model in the grid, and the best model for each object is selected. The best models were finally inspected visually by comparing them with the corresponding observed spectra. Due to the lower signal-to-noise ratio in the SSO 2.3 m spectra bluewards of 500 nm (see Fig. 3), especially for spectral types later than M4, we excluded this region below 500 nm from the χ^2 computation. We also checked the variation in effective

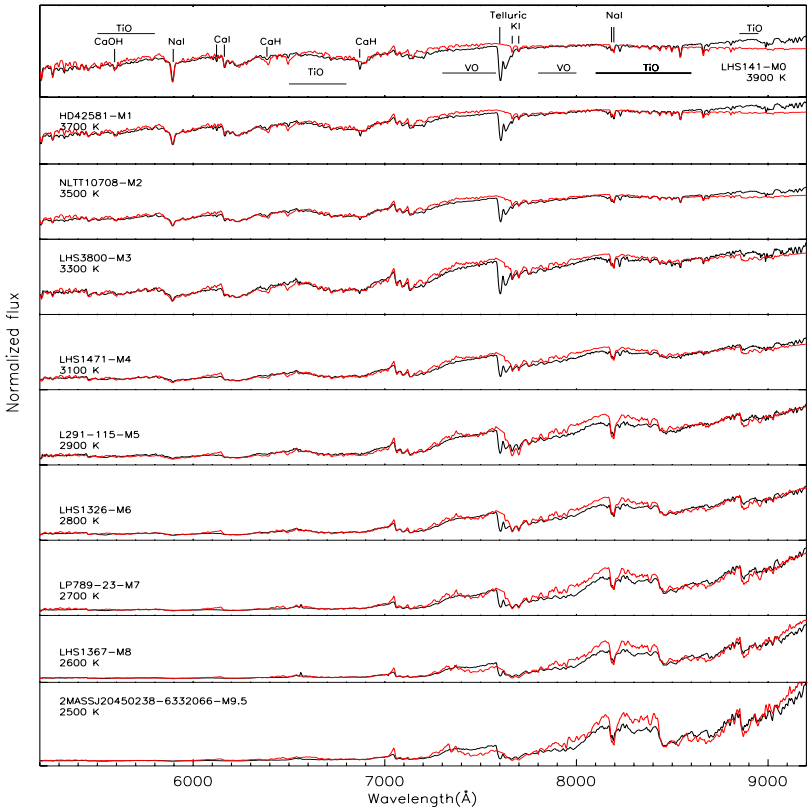

Fig. 2. Optical to red SED of M dwarfs from M0 to M9.5 observed with the NTT at a spectral resolution of 10.4 Å compared to the best fit BT-Settl synthetic spectra (red lines). The models displayed have a surface gravity of log g = 5.0 to 5.5. Telluric features near 7600 Å were ignored from the chi-square minimization.

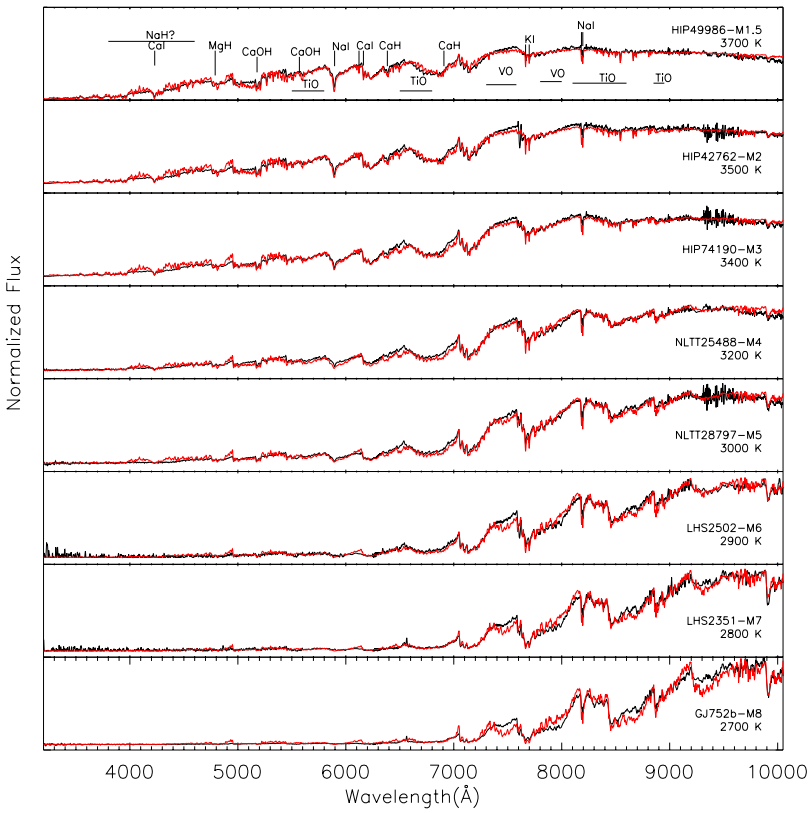

Fig. 3. Optical to red SED of M dwarfs from M1 to M8 observed with the SSO 2.3 m at a spectral resolution of 1.4 Å compared to the best fitting (chi-square minimization) BT-Settl synthetic spectra (red lines). The models displayed have a surface gravity of log g = 5.0 to 5.5. At blue wavelengths (<5000 Å) the instrumental noise dominates the late-type M dwarfs.

temperature of the best fit as a function of the spectral type of the observed dwarfs. We found generally good agreement and conclude that our model-fitting procedure can be used to estimate the effective temperature with an uncertainty of ∼100 K. The purpose of this fit is to determine the effective temperature by fitting the overall shape of the optical spectra. No attempt has been made to fit the individual atomic lines, such as the K I and Na I resonance doublets. With the available resolution we cannot constrain the metallicity, high-resolution spectra would be necessary (Rajpurohit et al. 2012a). In addition, we checked the influence of the spectral resolution on our derived temperatures. We degraded the resolution of the spectra of SSO 2.3 m down to 1 nm and redid the procedure. No systematic difference in $T_{\rm eff}$ was found. The results are summarized in Tables 1 and 2.

5. Comparison between models and observations

5.1. Spectroscopic confrontation

The optical spectrum of M dwarfs is dominated by molecular band absorption, leaving no window onto the continuum (Allard 1990). The major opacity sources in the optical regions are due to TiO and VO bands, as well as to MgH, CaH, FeH hydride bands and CAOH hydroxide bands in late-type M dwarfs. In M dwarfs of spectral type later than M6, the outermost atmospheric layers fall below the condensation temperature of silicates, giving rise to the formation of dust clouds (Tsuji et al. 1996a,b; Allard et al. 1997).

We compared the two samples of M dwarfs with the most recent BT-Settl synthetic spectra in Figs. 2 and 3 through the entire M dwarf spectral sequence. The synthetic spectra reproduce very well the slope of the observed spectra across the M dwarf regime. This is a drastic improvement compared to previous comparisons of earlier models (e.g., Leggett et al. 1998).

However, some indications of missing opacities persist in the blue part of the late-type M dwarf, such as the $B'^2\Sigma^+ < -X^2\Sigma^+$ system of MgH (Skory et al. 2003), and TiO and VO opacities around 8200 Å. Opacities are totally missing for the CaOH band at 5570 Å. The missing hydride bands of AlH and NaH between 3800 and 4600 Å among others could be responsible for the remaining discrepancies. We note that chromospheric emission fills the Na I D transitions in the latest type M dwarfs displayed here.

We see in this spectral regime no signs of dust scattering or of the weakening of features due to sedimentation onto grains until the M8 and later spectral types, where the spectrum becomes flat due to the sedimentation of TiO and VO bands and to the veiling by dust scattering.

5.2. Photometric confrontation

The models can be validated by comparing published isochrones interpolated into the new BT-Settl synthetic color tables with observed photometry. We took the $\log g$ and $T_{\rm eff}$ for the fixed age of 5 Gyr from Baraffe et al. (1998) isochrones and calculated the colors of the star according to the BT-Settl models. The models are compared to observations in color–color diagrams in Fig. 4 for our two samples. The compiled photometry in the NTT sample is less homogeneous and translates to a larger spread, in particular for colors including the V and R band. This dispersion becomes dramatic for the coolest and faintest stars except for lowest mass objects at very young ages. The isochrone reproduces the two samples over the entire M dwarf spectral range in most colors. In particular, the models reproduce

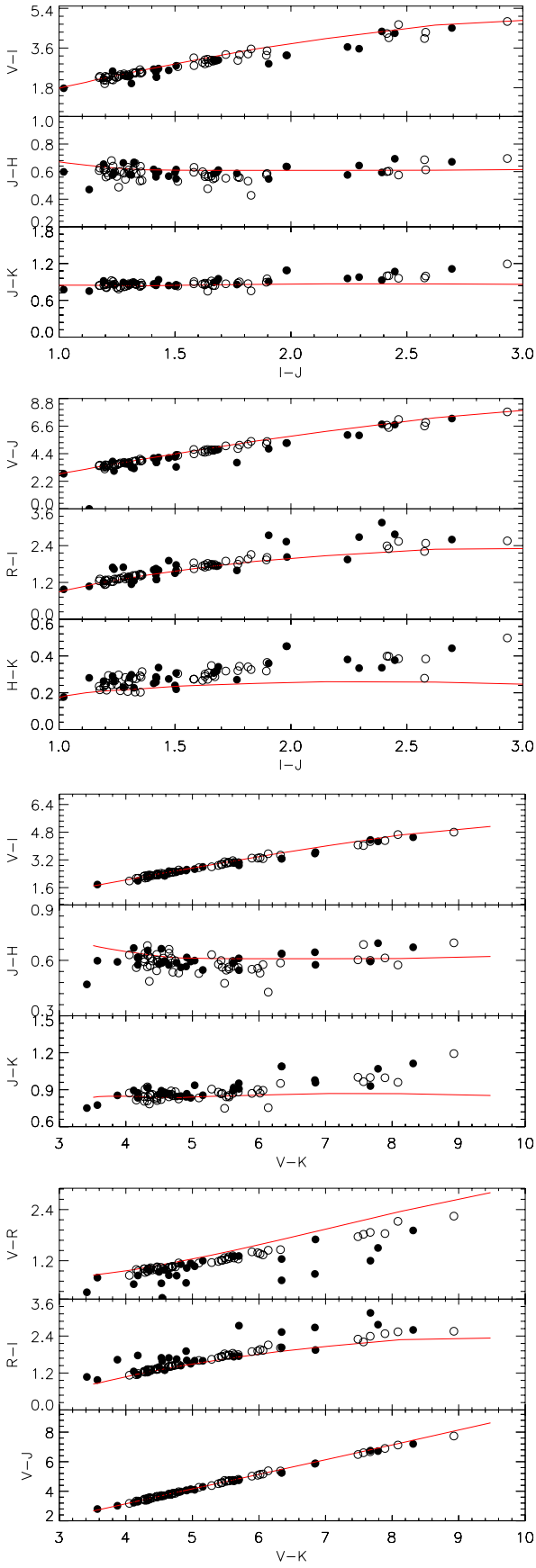

Fig. 4. Optical and NIR colors obtained with the 5 Gyr isochrones from Baraffe et al. (1998) at solar metallicity compared with the two observation samples (filled circles for the NTT sample and open circle for the SSO 2.3 m spectra). Typical error bars are comparable or smaller than the size of the symbols.

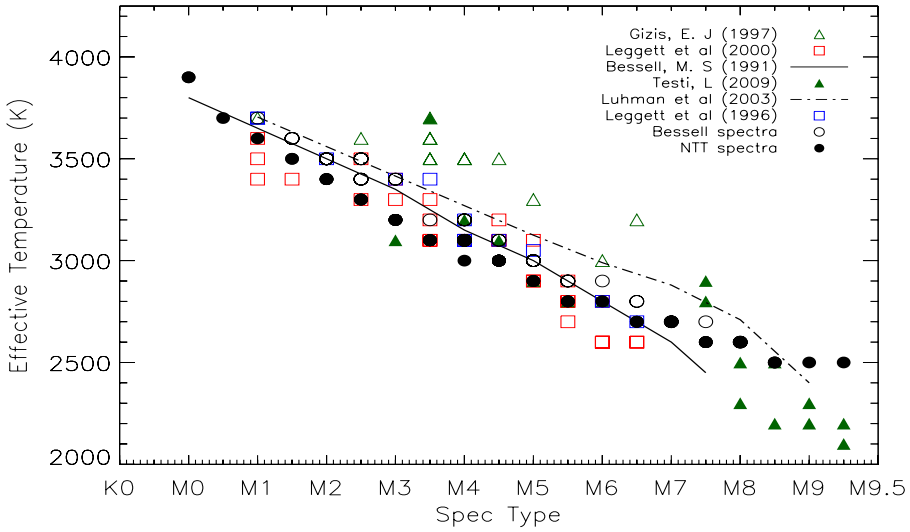

Fig. 5. Spectral type – $T_{\rm eff}$ relation obtained with the NTT sample (filled circles) and the SSO 2.3 m sample (open circles) compared to relations by Bessell (1991), Gizis (1997), Leggett et al. (1996), Leggett et al. (2000), Testi (2009), and Luhman et al. (2003).

the V-band colors of M dwarfs, as illustrated by the $V-I$, $V-J$, and $V-K$ colors. An increasing offset to the latest types persists in the $H-K$ and $V-R$ color indices. The observations also suggest a flattening and possibly a rise in $J-H$ and $J-K$ to the latest types, which is not reproduced by the model. These inadequacies at the coolest temperature could be linked to missing opacities.

5.3. The $T_{\rm eff}$ scale of M dwarfs

The effective temperature scale versus spectral type is shown in Fig. 5. The $T_{\rm eff}$ scale determined using the NTT sample (filled circles) is in agreement with the SSO sample (open circles), but we found systematically 100 K higher $T_{\rm eff}$ for SSO samples for spectral types later than M5. The relation shows a saturation trend for spectral types later than M8. This illustrates the fact that the optical spectrum no longer changes sensitively with $T_{\rm eff}$ in this regime due to dust formation.

In the following we compare our scale to other works. Bessell (1991) determined the temperatures by comparing blackbodies to the NIR photometry of their sample. They used the temperature calibration of Wing & Rinsland (1979) and Veeder (1974). These calibrations were identical between $2700 \leq T_{\rm eff} \leq 3500$ K. Their scale agrees with the modern values for M dwarfs earlier than M6, but becomes gradually too cool with later spectral types and too hot for earlier M types.

Leggett et al. (1996) used the base grid by Allard & Hauschildt (1995), which covers the range of parameters down to the coolest known M dwarfs, M subdwarfs, and brown dwarfs. They obtained the $T_{\rm eff}$ of M dwarfs by comparing the observed spectra to the synthetic spectra. They performed their comparison independently at each of their four wavelength regions: red, J, H, and K. The different wavelength regions gave consistent values of $T_{\rm eff}$ within 300 K. Gizis (1997) used the NextGen model atmosphere grid by Allard et al. (1997). These models include more molecular lines from ab initio simulations (in particular for water vapor) than the previous base model grid. Leggett et al. (2000) used the more modern AMES-Dusty model atmosphere grid by Allard et al. (2001). They obtained a revised $T_{\rm eff}$ scale which is 150–200 K cooler for early Ms and 200 K hotter for late Ms than the scale presented in Fig. 5. Testi (2009) determined the $T_{\rm eff}$ by fitting the synthetic spectra to the observations. They used three classes of models: the AMES-Dusty, AMES-Cond, and the BT-Settl models. With some individual exceptions they found that the BT-Settl models were the most appropriate for M type and early L-type dwarfs.

Finally, for spectral types later than M0, Luhman et al. (2003) adopted the effective temperature, which is based on the NextGen and AMES-Dusty evolutionary models of Baraffe et al. (1998) and Chabrier et al. (2000), respectively. They obtained the $T_{\rm eff}$ by comparing the H-R diagram from theoretical isochrones of Baraffe et al. (1998) and Chabrier et al. (2000). For M8 and M9, Luhman et al. (2003) adjusted the temperature scale from Luhman (1999), so that spectral sequence falls parallel to the isochrones. Their $T_{\rm eff}$ conversion is likely to be inaccurate at some level, but as it falls between the scales for dwarfs and giants, the errors in $T_{\rm eff}$ are modest.

The different $T_{\rm eff}$ scales are in agreement within 250–300 K. But the Gizis (1997) relation shows the largest differences with the largest $T_{\rm eff}$-values (up to 500 K). This is due to the incompleteness of the TiO and water vapor line lists used in the NextGen model atmospheres. We also note also how the Luhman et al. (2003) $T_{\rm eff}$ scale is gradually overestimating $T_{\rm eff}$ towards the bottom of the main sequence for spectral types later than M4.

$T_{\rm eff}$ versus color relations are shown in Fig. 6 in various photometric bands. The photometry of our NTT sample (filled circles) is compiled from the literature, which causes a large spread, particularly in the V and R band. The SSO 2.3 m sample (open circles) in comparison is more uniform. Our relations are compared to the predictions from BT-Settl isochrones at 5 Gyr. The relations show that the model is able to reproduce quite properly the colors of M dwarfs, even in the V-band. There is a slight offset visible in the R band due to missing molecular opacities (see above). These relations are compared to previously published relations when available.

Berriman et al. (1992) derive the $T_{\rm eff}$ by matching the blackbody flux anchored at K band (2.2 μm) to the total bolometric flux, including both the spectroscopic and photometric observed data points. They estimated the uncertainties in $T_{\rm eff}$ to be ±4%. Leggett et al. (1996) used the synthetic $I-K$ and $I-J$ colors to estimate $T_{\rm eff}$. Leggett et al. (1996) used synthetic broadband colors from the preliminary version of AMES-Dusty model produced by Allard et al. (1994). They used the $V-K$, $I-K$, $J-H$, and $H-K$ colors assuming $\log g = 5.0$ and solar metallicity, finding a hotter $T_{\rm eff}$ scale (by on average 130 K) than that of Berriman et al. (1992). More recently, Casagrande et al. (2008) used the PHOENIX Cond-GAIA model atmosphere grid (Hauschildt, unpublished) to determine the atmospheric parameters of their

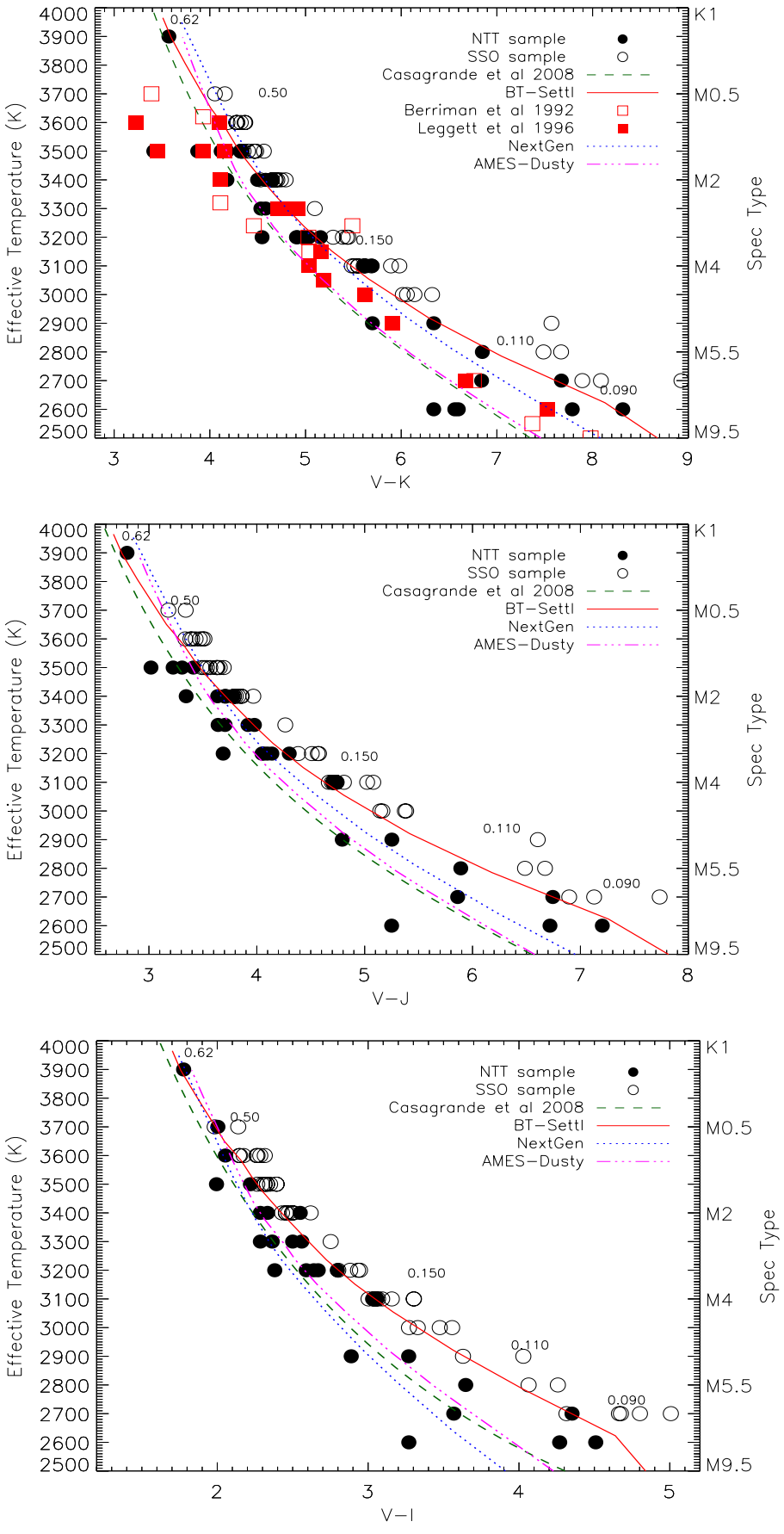

Fig. 6. Colored $T_{\rm eff}$ plots in different bands from the NTT sample (filled circles) and the SSO 2.3 m sample (open circles). Spectral types are also indicated. The predictions from BT-Settl (solid line), NextGen (dotted line), and AMES-Dusty (dash-dotted) for solar metallicities are over plotted. Theoretical masses in solar mass are indicated. Predictions from other authors are shown for comparison when available.

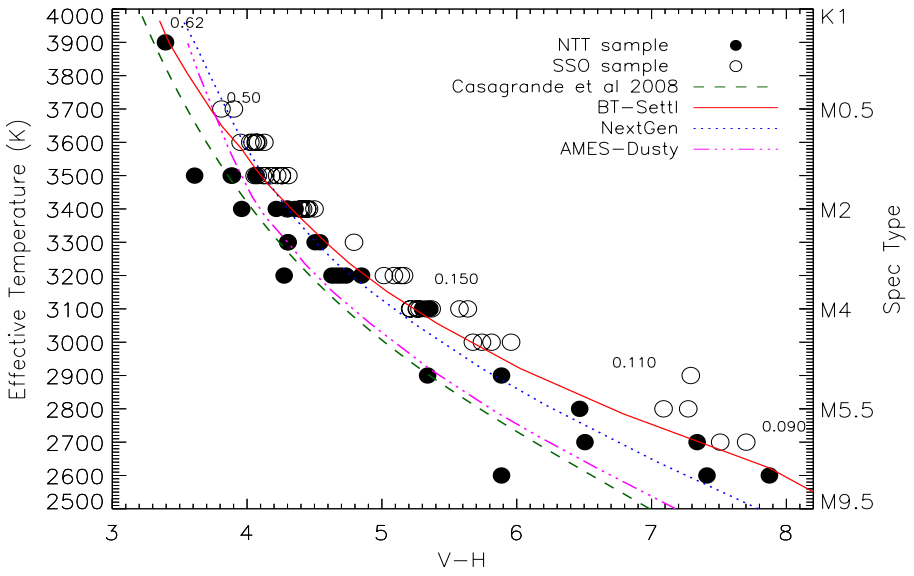

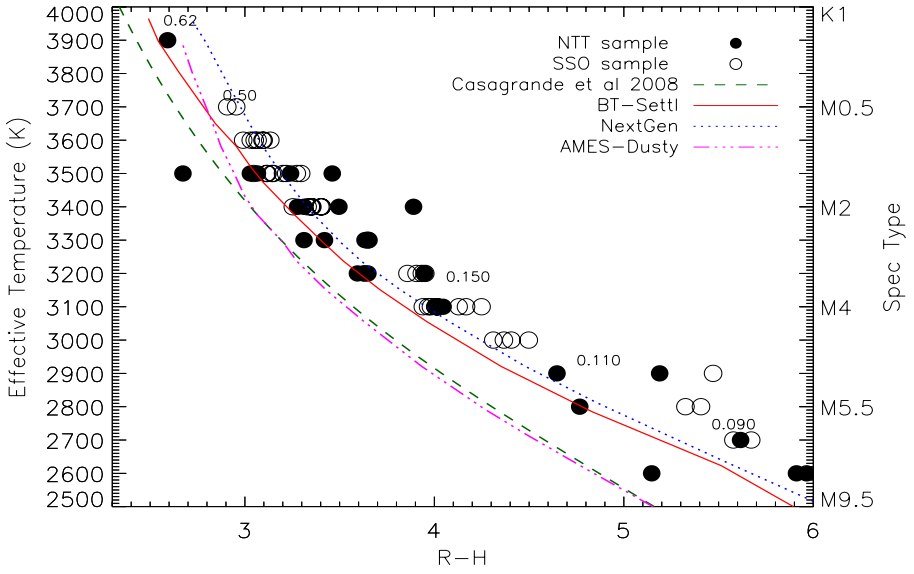

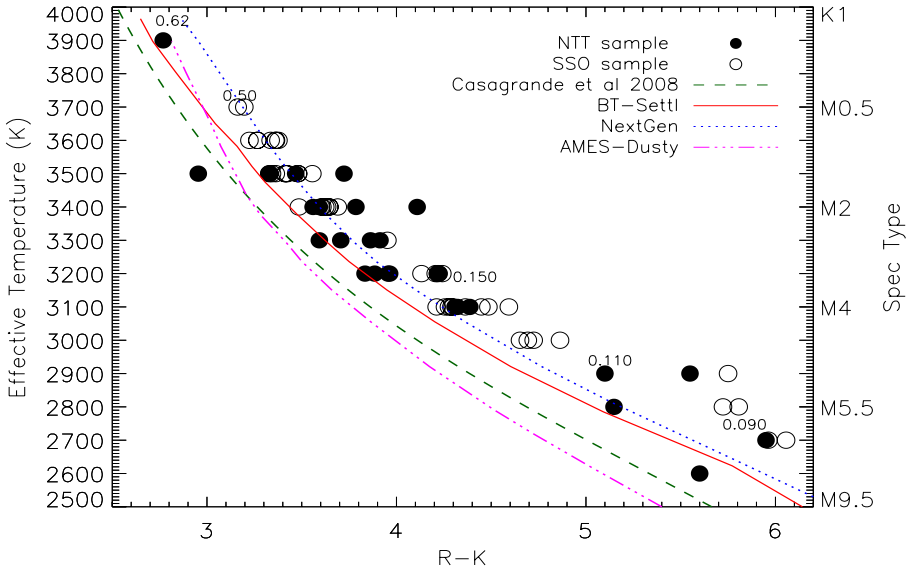

Fig. 6. continued.

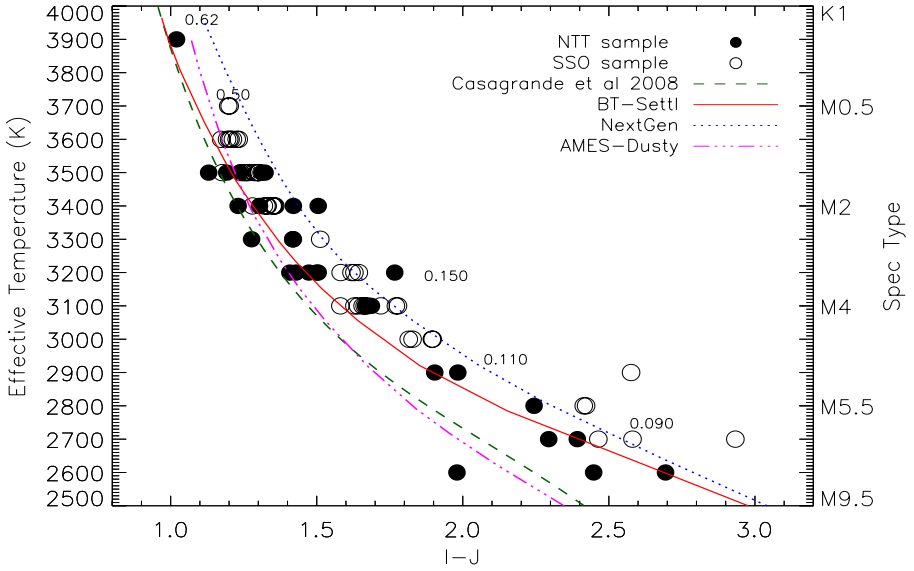

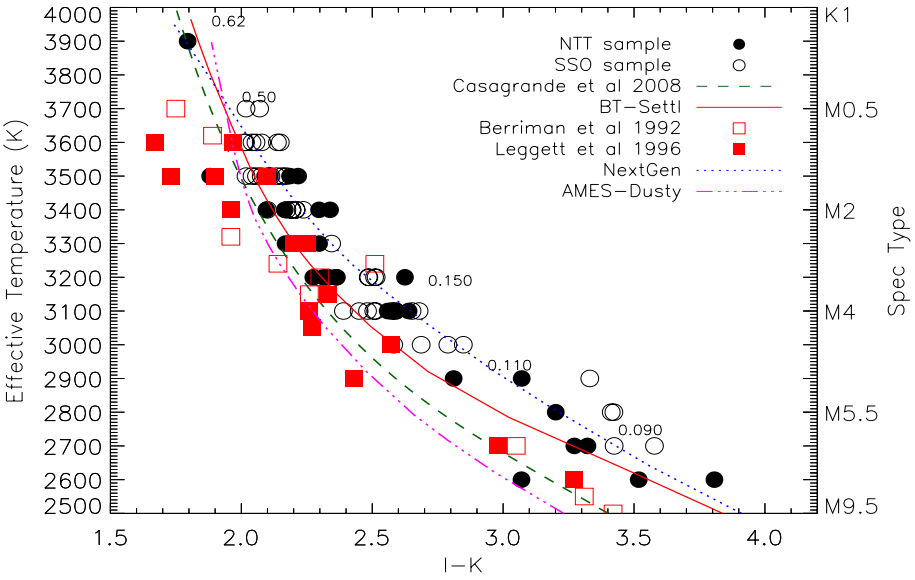

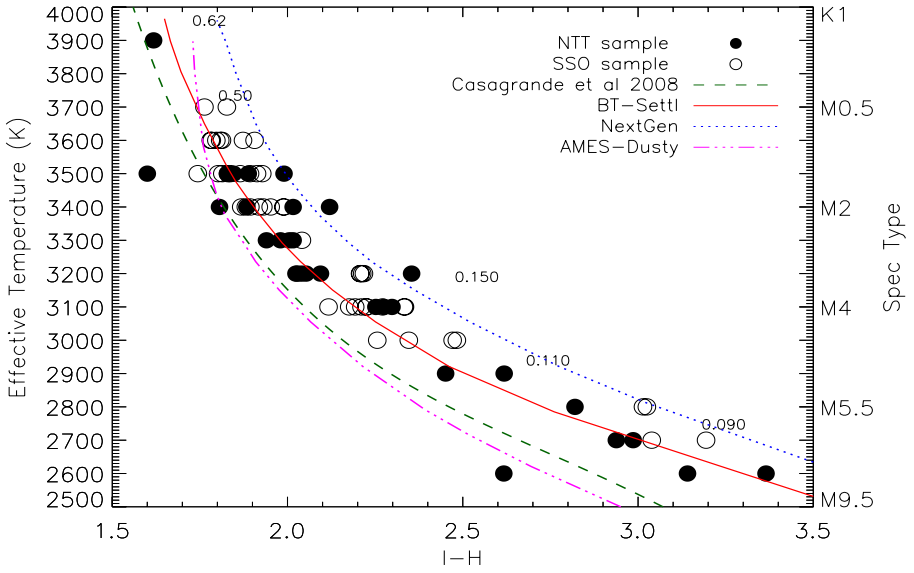

Fig. 6. continued.

sample of 343 nearby M dwarfs with high-quality optical and NIR photometry. These models are similar to those published by Allard et al. (2001), with the exception that they were computed by solving the radiative transfer in spherical symmetry. The authors determined the $T_{\rm eff}$ using a version of the multiple optical-infrared method (IRFM) generalized to M dwarfs, and elaborated by Blackwell & Shallis (1977) and Blackwell et al. (1979, 1980). Figure 6 shows that the Casagrande et al. (2008) $T_{\rm eff}$ scale is systematically, and progressively with decreasing $T_{\rm eff}$, cooler than the BT-Settl isochrones. Given that a large number of stars are common with Casagrande et al. (2008) sample, we did a star-by-star comparison of the $T_{\rm eff}$ determination. The values are given in Tables 1 and 2. The comparison confirms the systematic offset in the temperature scale. For cooler stars with $T_{\rm eff} < 3000$ K, the $T_{\rm eff}$ determinations diverge by 100 to 300 K. This is due, among other things, to the use of the Grevesse et al. (1993) solar elemental abundances (see Allard et al. 2012, for a comparison of the different solar elemental abundance determinations and their effects on model atmospheres).

6. Conclusion

We have compared a revised version of the BT-Settl model atmospheres (Allard et al. 2012a) to the observed NTT and SSO 2.3 m spectra and colors. This new version uses the Caffau et al. (2011) solar elemental abundances, updates to the atomic and molecular line broadening, and the TiO line list from Plez (1998) and Plez (priv. comm.). This list provides a more accurate description of the TiO bands in the M dwarfs. The systematic discrepancy between the delta and epsilon bands found by Reiners (2005), which seriously affected the effective temperature determination, is largely alleviated by using the Plez (1998) and Plez (priv. comm.) TiO line list although discrepancies remain for the coolest stars. The BT-Settl models reproduce the SED and observed colors across the M dwarfs' spectral regime in unprecedented quality, as well as the colors. The V band is also well reproduced by the models. Discrepancies remain in the strength of some molecular absorption bands while other absorption bands are missing, in particular in the blue spectral range.

Effective temperatures were determined by using a least-square minimization routine, which gives accurate temperatures within 100 K uncertainty. We compared our temperature color to relations using multi-wavelength photometry with the predictions from BT-Settl isochrones, assuming an age of 5 Gyr. In general, the BT-Settl isochrones are in good agreement with the observed colors, even at temperatures below 2800 K affected by dust treatment in the BT-Settl models. We found that the Casagrande et al. (2008) $T_{\rm eff}$ scale is systematically cooler than the BT-Settl isochrones due, among other things, to the Grevesse et al. (1993) solar elemental abundances adopted in the GAIA-Cond model atmosphere grid used for that work. In contrast the Luhman et al. (2003) $T_{\rm eff}$ scale is progressively too hot towards the bottom of the main sequence. New interior and evolution models based on the BT-Settl models are currently being prepared.

We provide and compare temperature versus color relations in the optical and infrared, which match well the BT-Settl isochrones and can be further used for large photometric datasets. We determined the effective temperature scale for the M dwarfs in our samples. It extended down to the latest type of M dwarfs, where the dust cloud begins to form in their atmosphere.

Acknowledgements. The use of Simbad and Vizier databases at CDS as well as the ARICNS database were very helpful for this research. The research leading to these results has received funding from the French Agence Nationale de la Recherche, the Programme National de Physique Stellaire of CNRS (INSU), and the European Research Council under the European Community's Seventh Framework Programme (FP7/2007-2013 Grant Agreement no. 247060). It was also conducted within the Lyon Institute of Origins under grant ANR-10-LABX-66. The computations were performed at the Pôle Scientifique de Modélisation Numérique (PSMN) at the École Normale Supérieure in Lyon, and at the Gesellschaft für Wissenschaftliche Datenverarbeitung Göttingen in collaboration with the Institut für Astrophysik Göttingen.

References

Abel, M., Frommhold, L., Li, X., & Hunt, K. L. C. 2011, in 66th International Symposium On Molecular Spectroscopy
Allard, F. 1990, Ph.D. Thesis (Heidelberg: Ruprecht Karls Univ.)
Allard, F., & Hauschildt, P. H. 1995, ApJ, 445, 433
Allard, F., Hauschildt, P. H., Miller, S., & Tennyson, J. 1994, ApJ, 426, L39
Allard, F., Hauschildt, P. H., Alexander, D. R., & Starrfield, S. 1997, ARA&A, 35, 137
Allard, F., Hauschildt, P. H., Alexander, D. R., Tamanai, A., & Schweitzer, A. 2001, ApJ, 556, 357
Allard, N. F., Kielkopf, J. F., & Allard, F. 2007, Eur. Phys. J. D, 44, 507
Allard, F., Homeier, D., & Freytag, B. 2011, in ASP Conf. Ser., 448, eds. C. Johns-Krull, M. K. Browning, & A. A. West, 91
Allard, F., Homeier, D., & Freytag, B. 2012a, Roy. Soc. London Philos. Trans. Ser. A, 370, 2765
Allard, F., Homeier, D., Freytag, B., & Sharp, C. M. 2012b, in EAS Pub. Ser., eds. C. Reylé, C. Charbonnel, & M. Schultheis, 57, 3
Asplund, M., Grevesse, N., Sauval, A. J., & Scott, P. 2009, ARA&A, 47, 481
Bailey, J., & Kedziora-Chudczer, L. 2012, MNRAS, 419, 1913
Baraffe, I., Chabrier, G., Allard, F., & Hauschildt, P. H. 1998, A&A, 337, 403
Barber, R. J., Tennyson, J., Harris, G. J., & Tolchenov, R. N. 2006, MNRAS, 368, 1087
Barklem, P. S., Piskunov, N., & O'Mara, B. J. 2000, A&A, 363, 1091
Berriman, G., & Reid, N. 1987, MNRAS, 227, 315
Berriman, G., Reid, N., & Leggett, S. K. 1992, ApJ, 392, L31
Bessell, M. S. 1991, AJ, 101, 662
Bessell, M. S. 1995, in The Bottom of the Main Sequence – and Beyond, ed. C. G. Tinney, 123
Blackwell, D. E., & Shallis, M. J. 1977, MNRAS, 180, 177
Blackwell, D. E., Shallis, M. J., & Selby, M. J. 1979, MNRAS, 188, 847
Blackwell, D. E., Petford, A. D., & Shallis, M. J. 1980, A&A, 82, 249
Bochanski, J. J., Hawley, S. L., Covey, K. R., et al. 2010, AJ, 139, 2679
Bonfils, X., Mayor, M., Delfosse, X., et al. 2007, A&A, 474, 293
Bonfils, X., Gillon, M., Udry, S., et al. 2012, A&A, 546, A27
Borysow, A., Jørgensen, U. G., & Fu, Y. 2001, J. Quant. Spectr. Rad. Trans., 68, 235
Caffau, E., Ludwig, H.-G., Steffen, M., Freytag, B., & Bonifacio, P. 2011, Sol. Phys., 268, 255
Casagrande, L., & Schönrich, R. 2012, in Eur. Phys. J. Web Conf., 19, 5004
Casagrande, L., Flynn, C., & Bessell, M. 2008, MNRAS, 389, 585
Chabrier, G. 2003, PASP, 115, 763
Chabrier, G. 2005, in The Initial Mass Function 50 Years Later, eds. E. Corbelli, F. Palla, & H. Zinnecker, Astrophys. Space Sci. Lib., 327, 41
Chabrier, G., Baraffe, I., Allard, F., & Hauschildt, P. 2000, ApJ, 542, 464
Chowdhury, P. K., Merer, A. J., Rixon, S. J., Bernath, P. F., & Ram, R. S. 2006, Physical Chemistry Chemical Physics (Incorporating Faraday Transactions), 8, 822
Crifo, F., Phan-Bao, N., Delfosse, X., et al. 2005, A&A, 441, 653
Delfosse, X., Tinney, C. G., Forveille, T., et al. 1999, A&AS, 135, 41
Dulick, M., Bauschlicher, C. W., Jr., Burrows, A., et al. 2003, ApJ, 594, 651
Epchtein, N. 1997, in The Impact of Large Scale Near-IR Sky Surveys, eds. F. Garzon, N. Epchtein, A. Omont, B. Burton, & P. Persi, Astrophys. Space Sci. Libr., 210, 15
Freytag, B., Steffen, M., Ludwig, H.-G., et al. 2012, J. Comp. Phys., 231, 919
Gamache, R. R., Lynch, R., & Brown, L. R. 1996, J. Quant. Spec. Radiat. Transf., 56, 471
Gizis, J. E. 1996, in Cool Stars, Stellar Systems, and the Sun, eds. R. Pallavicini, & A. K. Dupree, ASP Conf. Ser., 109, 683
Gizis, J. E. 1997, AJ, 113, 806
Goorvitch, D., & Chackerian, C. Jr. 1994a, ApJS, 91, 483
Goorvitch, D., & Chackerian, C. Jr. 1994b, ApJS, 92, 311
Grevesse, N., Noels, A., & Sauval, A. J. 1993, A&A, 271, 587

Hauschildt, P. H., Baron, E., & Allard, F. 1997, ApJ, 483, 390
Hauschildt, P. H., Allard, F., & Baron, E. 1999, ApJ, 512, 377
Kirkpatrick, J. D., Kelly, D. M., Rieke, G. H., et al. 1993, ApJ, 402, 643
Koen, C., & Eyer, L. 2002, MNRAS, 331, 45
Koen, C., Kilkenny, D., van Wyk, F., & Marang, F. 2010, MNRAS, 403, 1949
Leggett, S. K., Allard, F., Berriman, G., Dahn, C. C., & Hauschildt, P. H. 1996, ApJS, 104, 117
Leggett, S. K., Allard, F., & Hauschildt, P. H. 1998, ApJ, 509, 836
Leggett, S. K., Allard, F., Dahn, C., et al. 2000, ApJ, 535, 965
Ludwig, H.-G., Allard, F., & Hauschildt, P. H. 2002, A&A, 395, 99
Ludwig, H.-G., Allard, F., & Hauschildt, P. H. 2006, A&A, 459, 599
Luhman, K. L. 1999, ApJ, 525, 466
Luhman, K. L., Stauffer, J. R., Muench, A. A., et al. 2003, ApJ, 593, 1093
Martín, E. L., Phan-Bao, N., Bessell, M., et al. 2010, A&A, 517, A53
Partridge, H., & Schwenke, D. W. 1997, J. Comp. Phys., 106, 4618
Pettersen, B. R. 1980, A&A, 82, 53
Phan-Bao, N., Martín, E. L., Reylé, C., Forveille, T., & Lim, J. 2005, A&A, 439, L19
Plez, B. 1998, A&A, 337, 495
Rajpurohit, A. S., Reylé, C., Schultheis, M., et al. 2012a, in SF2A-2012: Proc. Ann. meeting Fren. Soc. Astron. Astrophys., eds. S. Boissier, P. de Laverny, N. Nardetto, R. Samadi, D. Valls-Gabaud, & H. Wozniak, 383
Rajpurohit, A. S., Reylé, C., Schultheis, M., et al. 2012b, A&A, 545, A85
Reid, N., & Gilmore, G. 1984, MNRAS, 206, 19
Reid, I. N., & Gizis, J. E. 1997, AJ, 114, 1992
Reid, I. N., Cruz, K. L., Allen, P., et al. 2004, AJ, 128, 463
Reid, I. N., Cruz, K. L., & Allen, P. R. 2007, AJ, 133, 2825
Reiners, A. 2005, Astron. Nachr., 326, 930
Reylé, C., & Robin, A. C. 2004, A&A, 421, 643
Reylé, C., Robin, A. C., Scholz, R.-D., & Irwin, M. 2002, A&A, 390, 491
Reylé, C., Scholz, R.-D., Schultheis, M., Robin, A. C., & Irwin, M. 2006, MNRAS, 373, 705
Rossow, W. B. 1978, Icarus, 36, 1
Rothman, L. S., Gordon, I. E., Barbe, A., et al. 2009, J. Quant. Spec. Radiat. Transf., 110, 533
Skory, S., Weck, P. F., Stancil, P. C., & Kirby, K. 2003, ApJS, 148, 599
Skrutskie, M. F., Cutri, R. M., Stiening, R., et al. 2006, AJ, 131, 1163
Tashkun, S. A., Perevalov, V. I., Teffo, J.-L., et al. 2004, Proc. SPIE, 5311, 102
Testi, L. 2009, A&A, 503, 639
Tinney, C. G., & Reid, I. N. 1998, MNRAS, 301, 1031
Tinney, C. G., Mould, J. R., & Reid, I. N. 1993, AJ, 105, 1045
Tokunaga, A. T., & Kobayashi, N. 1999, AJ, 117, 1010
Tsuji, T., Ohnaka, K., & Aoki, W. 1996a, A&A, 305, L1
Tsuji, T., Ohnaka, K., Aoki, W., & Nakajima, T. 1996b, A&A, 308, L29
Udry, S., & Santos, N. C. 2007, ARA&A, 45, 397
Unsold, A. 1968, Physik der Sternatmospharen, MIT besonder Berucksichtigung der Sonne
Valenti, J. A., & Piskunov, N. 1996, A&AS, 118, 595
Veeder, G. J. 1974, AJ, 79, 1056
Weck, P. F., Schweitzer, A., Stancil, P. C., Hauschildt, P. H., & Kirby, K. 2003, ApJ, 584, 459
Wing, R. F., & Rinsland, C. P. 1979, AJ, 84, 1235
Witte, S., Helling, C., Barman, T., Heidrich, N., & Hauschildt, P. H. 2011, A&A, 529, A44
Yurchenko, S. N., Barber, R. J., & Tennyson, J. 2011, MNRAS, 413, 1828
Zacharias, N., Monet, D. G., Levine, S. E., et al. 2005, VizieR Online Data Catalog, I/297

Pages 12 to 14 are available in the electronic edition of the journal at http://www.aanda.org

Table 1. Observable and physical quantities for our sample of stars observed at NTT with EMMI.

Name	Spectral type	$T_{\rm eff}$ (K)	$T_{\rm eff}$[b] (K)	$\log g$ (cm s^{-2})	V	R	I	J	H	K
Gl143.1[a]	K7	3900	–	5.0	10.03	9.15	–	–	–	–
LHS141	M0	3900	–	5.0	10.15	9.35	8.38	7.36	6.76	6.58
LHS3833[a]	M0.5	3800	–	5.0	10.06	9.33	–	–	–	–
HD42581[a]	M1	3700	–	5.0	8.12	7.16	6.12	–	–	–
LHS14[a]	M1.5	3600	–	5.0	10.04	9.09	7.99	–	–	–
LHS65[a]	M1.5	3600	3567	5.0	10.86	10.31	10.64	–	–	–
L127-33	M2	3500	–	5.0	14.19	14.04	12.41	11.17	10.58	10.32
NLTT10708	M2	3500	–	5.0	11.16	10.31	9.17	7.86	7.28	6.98
LP831-68	M2	3500	–	5.0	11.02	10.02	8.80	7.61	6.95	6.69
NLTT83-11	M2	3500	–	5.0	12.90	12.25	11.00	9.68	9.01	8.78
APMPMJ0541-5349	M2	3500	–	5.0	13.30	12.84	11.77	10.64	10.17	9.89
LHS1656	M2.5	3400	–	5.0	13.30	12.44	10.75	9.52	8.94	8.65
LP763-82	M2.5	3400	–	5.0	12.19	11.25	9.86	8.55	7.97	7.69
LP849-55	M2.5	3400	–	5.0	13.32	13.25	11.48	9.97	9.36	9.14
LHS5090	M3	3300	–	5.0	–	14.97	12.85	11.58	11.04	10.84
LHS3800	M3	3300	–	5.0	–	–	12.23	10.93	10.39	10.15
LHS3842	M3	3300	–	5.0	13.80	12.95	11.30	9.88	9.29	9.04
LHS1293	M3	3300	–	5.0	13.65	12.66	11.36	9.94	9.35	9.07
LP994-114	M3	3300	–	5.0	–	11.59	10.36	9.00	8.37	8.15
LTT9783	M3	3300	–	5.0	–	12.11	10.56	9.17	8.59	8.34
LP715-39	M3	3300	3161	5.0	12.65	11.53	10.09	8.67	8.11	7.82
LHS1208[a]	M3	3300	–	5.0	9.85	8.97	–	–	–	–
LEHPM4417	M3	3300	–	5.0	13.73	13.06	11.37	10.09	9.43	9.20
LP831-45	M3.5	3200	3125	5.0	12.54	11.51	9.90	8.49	7.88	7.62
2MASS J04060688-0534444	M3.5	3200	–	5.0	13.29	12.28	–	9.13	8.55	8.30
LP834-32	M3.5	3200	3108	5.0	12.38	11.24	9.74	8.24	7.65	7.41
LHS502[a]	M3.5	3200	–	5.0	11.49	10.43	9.11	–	–	–
LEHPM 1175	M3.5	3200	–	5.0	–	13.08	11.51	10.01	9.47	9.17
LEHPM1839	M3.5	3200	–	5.0	–	13.32	12.11	10.55	9.95	9.71
L130-37	M3.5	3200	–	5.0	13.04	11.97	10.37	8.94	8.34	8.01
LEHPM6577	M3.5	3200	–	5.0	–	13.03	11.79	10.34	9.73	9.47
L225-57	M4	3200	–	5.0	–	11.70	9.79	8.23	7.61	7.31
LP942-107	M4	3200	3052	5.0	13.93	12.73	11.13	9.63	9.08	8.77
LP772-8	M4	3200	–	5.0	14.11	13.43	11.52	10.05	9.48	9.20
LP1033-31	M4	3200	–	5.0	–	12.12	10.54	9.10	8.46	8.21
L166-3	M4	3200	–	5.0	–	12.76	11.33	9.83	9.28	9.00
LP877-72	M4	3200	–	5.0	–	11.–	10.22	8.86	8.24	8.00
LP878-73	M4	3200	–	5.0	14.55	14.22	12.63	10.86	10.27	10.00
LP987-47	M4	3200	–	5.0	–	–	10.82	9.41	8.78	8.55
LP832-7	M4	3200	–	5.0	14.09	13.45	–	9.87	9.24	8.98
LHS183	M4	3200	–	5.0	12.79	11.51	–	8.57	8.00	7.75
LHS1471	M4	3200	–	5.0	–	13.22	11.56	9.94	9.37	9.08
APMPMJ2101-4125	M4	3200	–	5.0	–	13.34	11.47	9.96	9.38	9.09
APMPMJ2101-4907	M4	3200	–	5.0	–	–	10.52	9.12	8.48	8.19
LEHPM3260	M4	3200	–	5.0	–	12.53	10.60	9.13	8.54	8.19
LEHPM3866	M4	3200	–	5.0	–	–	11.82	10.21	9.58	9.29
LEHPM5810	M4	3200	–	5.0	–	13.58	11.66	9.91	9.33	9.05
LHS5045	M4.5	3100	–	5.0	–	–	10.78	9.17	8.60	8.24
LP940-20	M4.5	3100	–	5.0	–	14.87	12.65	10.92	10.32	10.01
L170-14A	M4.5	3100	–	5.0	–	12.86	11.50	9.76	9.13	8.88

Notes. [(a)] Saturation in NIR bands. [(b)] $T_{\rm eff}$ from Casagrande et al. (2008).

Table 1. continued.

Name	Spectral type	$T_{\rm eff}$ (K)	$T_{\rm eff}{}^{b}$ (K)	$\log g$ (cm s^{-2})	V	R	I	J	H	K
LHS1201	M4.5	3100	–	5.0	17.55	15.52	12.90	11.12	10.52	10.25
LHS1524	M4.5	3100	–	5.0	–	14.45	12.65	10.98	10.45	10.17
LTT1732	M4.5	3100	–	5.0	–	13.19	11.27	9.69	9.11	8.80
LP889-37	M4.5	3100	2923	5.0	14.52	13.21	11.46	9.77	9.16	8.82
LHS5094	M4.5	3100	–	5.0	14.02	12.72	10.97	9.30	8.72	8.41
LP655-43	M4.5	3100	2924	5.0	14.44	13.14	11.41	9.73	9.14	8.82
LHS138[a]	M4.5	3100	–	5.0	12.07	10.70	8.94	–	–	–
APMPMJ1932-4834	M4.5	3100	–	5.0	–	14.38	12.37	10.63	10.02	9.72
2MASS J23522756-3609128	M4.5	3100	–	5.0	–	17.27	–	13.09	12.57	12.28
LEHPM640	M4.5	3100	–	5.0	17.74	14.26	12.30	10.76	10.14	9.90
LEHPM1853	M4.5	3100	–	5.0	–	12.77	11.03	9.46	8.85	8.61
LEHPM3115	M4.5	3100	–	5.0	–	13.94	12.10	10.49	9.92	9.63
LEHPM4771	M4.5	3100	–	5.0	17.74	13.79	11.29	9.54	8.95	8.63
LEHPM4861	M4.5	3100	–	5.0	–	13.28	11.75	10.13	9.60	9.34
L291-115	M5	2900	–	5.0	15.88	14.90	12.26	10.44	9.83	9.54
LP904-51	M5	2900	–	5.0	–	15.32	12.84	11.04	10.44	10.16
LHS168	M5	2900	–	5.0	13.78	12.60	–	8.77	8.21	7.83
LP829-41	M5.5	2800	–	5.0	16.10	15.95	13.21	11.31	10.76	10.40
LP941-57	M5.5	2800	–	5.0	–	14.88	12.98	11.06	10.47	10.13
LHS546	M5.5	2800	–	5.0	14.69	–	–	9.15	8.50	8.18
LP714-37	M5.5	2800	–	5.5	16.26	15.02	12.99	11.01	10.37	9.92
LHS1326	M6	2800	–	5.5	15.61	14.49	–	9.84	9.25	8.93
2MASS J12363959-1722170	M6	2800	–	5.0	17.56	15.86	13.91	11.67	11.09	10.71
2MASS J21481595-1401059	M6.5	2700	–	5.0	–	20.20	17.15	14.68	14.11	13.65
2MASS J05181131-3101519	M6.5	2700	–	5.0	17.74	16.85	14.17	11.88	11.23	10.90
LP788-1	M6.5	2700	–	5.0	–	16.66	13.36	11.07	10.47	10.07
APMPMJ1251-2121	M6.5	2700	–	5.0	–	16.65	13.78	11.16	10.55	10.13
APMPMJ2330-4737	M7	2700	–	5.0	–	–	13.70	11.23	10.64	10.28
LP789-23	M7	2700	–	5.0	–	17.90	14.55	12.04	11.39	10.99
LHS292	M7	2700	–	5.5	15.60	14.40	11.25	8.86	8.26	7.93
2MASS J03144011-0450316	M7.5	2600	–	5.0	–	19.43	–	12.64	12.00	11.60
LHS1604	M7.5	2600	–	5.0	18.02	16.52	13.75	11.30	10.61	10.23
LP714-37	M7.5	2600	–	5.5	16.26	15.52	12.99	11.01	10.37	9.92
LP655-48	M7.5	2600	2250	5.0	17.86	15.95	13.35	10.66	9.99	9.54
LP851-346	M7.5	2600	–	5.5	–	16.79	13.77	10.93	10.29	9.88
LHS1367	M8	2600	–	5.0	–	17.34	14.18	11.62	10.95	10.54
2MASS J05022640-0453583	M8	2600	–	5.0	–	20.39	17.35	14.52	13.95	13.58
LHS132	M8	2600	–	5.0	–	17.14	13.83	11.13	10.48	10.07
2MASS J22062280-2047058	M8	2600	–	5.0	–	18.93	15.09	12.37	11.69	11.31
2MASS J22264440-7503425	M8	2600	–	5.0	–	18.95	15.20	12.35	11.70	11.25
2MASS J04103617-1459269	M8.5	2500	–	5.5	–	–	16.68	13.94	13.24	12.81
2MASS J05084947-1647167	M8.5	2500	–	5.5	–	–	16.46	13.69	12.96	12.53
2MASS J04362788-4114465	M8.5	2500	–	5.5	–	19.96	16.04	13.10	12.43	12.05
2MASS J10481463-3956062	M9	2500	–	5.5	–	15.93	12.67	9.54	8.90	8.45
2MASS J20450238-6332066	M9.5	2500	–	5.5	–	19.24	16.05	12.62	11.81	11.21
2MASS J09532126-1014205	M9.5	2500	–	5.5	–	19.58	16.82	13.47	12.64	12.14

Table 2. Observable and physical quantities for our sample of stars observed at SSO.

Name	Spectral type	$T_{\rm eff}$ (K)	$T_{\rm eff}{}^{b}$ (K)	log g (cm s^{-2})	V	R	I	J	H	K
HIP 49986	M1.5	3700	3445	5.0	9.07	8.21	7.08	5.89	5.26	5.01
HIP 82256	M1.5	3700	3470	5.0	11.38	10.39	9.24	8.04	7.48	7.22
HIP 56528	M1.5	3600	3472	5.0	9.81	8.85	7.66	6.47	5.86	5.62
NLTT19190	M1.5	3600	3456	5.0	11.49	10.57	9.34	8.11	7.47	7.20
NLTT42523	M2	3600	3444	5.0	12.08	11.06	9.81	8.60	8.01	7.80
HIP 80229	M2	3600	3486	5.0	11.91	10.90	9.65	8.48	7.87	7.64
LP725-25	M2	3600	3476	5.0	11.76	10.82	9.59	8.36	7.68	7.44
HIP 61413	M2	3500	3454	5.0	11.49	10.48	9.17	7.99	7.37	7.15
LP853-34	M2	3500	3339	5.0	12.32	11.31	9.99	8.69	8.10	7.83
LP859-11	M2	3500	3433	5.0	12.00	10.97	9.69	8.49	7.88	7.63
LP788-49	M2	3500	3356	5.0	11.81	10.85	9.55	8.30	7.74	7.49
HIP 42762	M2	3500	3302	5.0	11.75	10.76	9.42	8.12	7.49	7.28
HIP 51317	M2	3500	3403	5.0	9.67	8.67	7.34	6.18	5.60	5.31
HIP 60559	M2	3500	3382	5.0	11.30	10.29	8.99	7.73	7.25	6.95
HIP 47103	M2	3500	3319	5.0	10.87	9.89	8.58	7.34	6.74	6.47
HIP 93206	M2.5	3500	3366	5.0	11.23	10.18	8.80	7.52	6.93	6.70
LP834-3	M2.5	3500	–	5.0	–	–	–	–	–	–
HIP 84521	M2.5	3500	3345	5.0	11.57	10.53	9.22	7.93	7.39	7.11
HIP 91430	M2.5	3500	3352	5.0	11.32	10.26	8.92	7.66	7.06	6.85
HIP 50341	M2.5	3500	3314	5.0	11.02	10.01	8.62	7.32	6.71	6.45
LP672-2	M2.5	3400	–	5.0	12.58	11.54	10.12	8.80	8.14	7.93
NLTT24892	M2.5	3400	3244	5.0	12.52	11.47	10.05	8.73	8.118	7.84
NLTT34577	M2.5	3400	3254	5.0	12.44	11.40	9.99	8.64	8.00	7.80
LP670-17	M3	3400	3226	5.0	12.14	11.08	9.63	8.28	7.68	7.39
HIP 59406	M3	3400	3226	5.0	11.75	10.69	9.25	7.89	7.36	7.04
HIP 74190	M3	3400	3258	5.0	11.55	10.48	9.05	7.72	7.13	6.86
NLTT46868	M3.5	3400	3221	5.0	12.23	11.08	9.61	8.26	7.73	7.44
HIP 62452	M4	3300	3095	5.0	11.46	10.31	8.71	7.19	6.67	6.36
NLTT25488	M4	3200	2986	5.0	15.66	14.46	12.73	11.09	10.52	10.21
NLTT29087	M4	3200	2971	5.0	14.79	13.57	11.84	10.22	9.62	9.35
NLTT29790	M4	3200	2987	5.0	14.73	13.54	11.85	10.22	9.64	9.34
LP734-32	M4	3200	3024	5.0	12.15	10.99	9.35	7.77	7.14	6.86
LP739-2	M4	3100	2939	5.0	14.44	13.18	11.40	9.73	9.17	8.89
LP735-29	M4	3100	2940	5.0	14.18	12.95	11.18	9.52	8.97	8.67
GJ1123	M4	3100	–	5.0	13.14	11.90	10.10	8.33	7.77	7.45
GJ1128	M4	3100	–	5.0	12.66	11.40	9.61	7.95	7.38	7.04
NLTT35266	M4.5	3100	2942	5.0	15.15	13.88	12.05	10.41	9.94	9.66
NLTT41951	M4.5	3100		5.0	15.06	13.77	11.99	10.36	9.80	9.51
NLTT21329	M4.5	3000	2949	5.0	13.75	12.38	10.42	8.60	8.07	7.73
LP732-35	M5	3100	2901	5.0	14.10	12.78	10.94	9.36	8.76	8.49
NLTT18930	M5	3100	2903	5.0	15.34	13.93	12.03	10.31	9.76	9.44
2MASS J14221943-7023371	M5	3000	–	5.0	–	–	–	–	–	–
NLTT22503	M5	3000	2785	5.0	13.66	12.32	10.39	8.50	7.92	7.60
NLTT28797	M5	3000	2826	5.0	15.62	14.24	12.32	10.54	9.99	9.64
NLTT30693	M5.5	3000	2785	5.5	15.32	13.86	11.85	9.95	9.36	9.00
LHS288	M5.5	3000	2770	5.0	13.87	12.42	10.31	8.48	8.05	7.73
GJ551	M5.5	2900	–	5.0	3.63	2.08	5.36	4.83	4.38	–
LHS2502	M6	2900	2468	5.5	19.36	17.54	15.33	12.75	12.07	11.79
NLTT20726	M6.5	2800	2464	5.0	16.11	14.24	11.85	9.44	8.84	8.44
GJ406	M6.5	2800	–	5.5	13.57	11.81	9.51	7.08	6.48	6.08
LHS2351	M7	2800	2346	5.5	19.22	17.39	14.91	12.33	11.72	11.33
SCR J1546-5534	M7.5	2700	–	5.5	–	–	–	–	–	–
GJ752b	M8	2700	–	5.5	5.01	–	–	9.91	9.23	8.76
GJ644c	M7	2700	–	5.5	16.90	14.78	12.24	9.78	9.20	8.82
LHS2397a	M8	2700	–	5.5	19.66	17.42	14.86	11.93	11.23	10.73

Notes. [(b)] $T_{\rm eff}$ from Casagrande et al. (2008).